Chapter 10
Bond Graph Modelling of a Solid Oxide Fuel Cell

P. Vijay, A.K. Samantaray, and A. Mukherjee

Abstract Fuel cells are environmentally friendly futuristic power sources. They involve multiple energy domains and hence bond graph method is suitable for their modelling. A true bond graph model of a solid oxide fuel cell is presented in this chapter. This model is based on the concepts of network thermodynamics, in which the couplings between the various energy domains are represented in a unified manner. The simulations indicate that the model captures all the essential dynamics of the fuel cell and therefore is useful for control theoretic analysis.

Keywords Solid oxide fuel cell · Bond graph · Network thermodynamics · Electrochemical reaction · Fuel utilization

Notation

A_c	Effective cell area (m^2)
c_p, c_v	Specific heat capacity at constant pressure and volume (J kg^{-1} K^{-1})
E	Activation energy (J mol^{-1})
F	Faraday's constant (C mol^{-1})
G	Gibbs free energy (J)
h	Specific enthalpy (J kg^{-1})
H	Enthalpy (J)
i	Current (A)
K	Valve coefficient (m s)
m	Mass (kg)
$\dot{m}$	Mass flow rate (kg s^{-1})
M	Molar mass (g)
n	Number of moles (mol)
n_e	Number of electrons participating in the reaction

P. Vijay (✉)
Department of Chemical Engineering, Curtin University of Technology, Perth, WA 6845, Australia
e-mail: vijay103@rediffmail.com

W. Borutzky (ed.), *Bond Graph Modelling of Engineering Systems*,
DOI 10.1007/978-1-4419-9368-7_10,

p	Pressure (N m^{-2})
R	Specific gas constant (J kg^{-1} K^{-1})
R	Universal gas constant (J mol^{-1} K^{-1})
s	Specific entropy (J kg^{-1} K^{-1})
S	Entropy (J K^{-1})
$\dot{S}$	Entropy flow rate (J $K^{-1}s^{-1}$)
T	Temperature (K)
u	Specific internal energy (J kg^{-1})
U	Internal energy (J)
v	Specific volume (m^3 kg^{-1})
V	Volume (m^3)
$\dot{V}$	Volume flow rate (m^3 s^{-1})
w	Mass fraction
x	Valve stem position (m)
ν	Stoichiometric coefficient
η	Over-voltage (V)
μ	Chemical potential (J kg^{-1})
ψ	Pre-exponential coefficient (A m^{-2})
ξ	Reaction advancement coordinate (mol)
ζ_f, ζ_o	Fuel and oxygen utilisations
β	Charge transfer coefficient
λ	Convection heat trans. coefficient (J m^{-2} s^{-1} K^{-1})

Subscripts

ai	Anode side inlet
an	Anode
ao	Anode side outlet
act	Activation
AS	Air source
b	Bulk
ca	Cathode
ci	Cathode side inlet
co	Cathode side outlet
conc	Concentration
d	Downstream side
ENV	Environment
gen	Generated
H	Hydrogen gas
HS	Hydrogen source
I1	Interconnect on anode side
I2	Interconnect on cathode side
L	Limiting
M	Membrane electrode assembly

N	Nitrogen gas
ohm	Ohmic
O	Oxygen gas
PL	Polarisation losses
r	Reaction
TPB	Triple phase boundary
u	Upstream side
W	Water vapour

Superscripts

i	Inlet
o	Outlet
r	Reaction
ref	Reference state
0	Initial state

10.1 Introduction

The ever-increasing energy requirements of mankind and rapidly depleting natural resources combined with the detrimental effects of increased atmospheric pollution have motivated scientists and engineers to develop cleaner and more efficient energy conversion mechanisms. In this context, fuel cells, which are efficient and environmentally friendly power-generating systems that produce electrical energy by combining fuel and oxygen electrochemically, are alternatives worthy of consideration. Fuel cell research is attracting much greater effort and attention today than ever before in its long history.

A fuel cell is an energy conversion device where the reactants are continuously supplied and the products are continuously removed. The electrodes and electrolyte do not participate in the chemical reaction but they provide the surfaces on which the reactions take place and they also serve as conductors for the electrons and ions. Therefore, a fuel cell can be defined as a thermo-electrochemical device, which converts chemical energy from the reaction of a fuel with an oxidant directly and continuously into electrical energy.

The basic components of a general fuel cell are two porous electrodes, i.e. anode and cathode, which are separated by a solid or liquid electrolyte. The electrolyte is impervious to gases. Fuel is supplied to the anode side and air is supplied to the cathode side. The oxidation reaction is made possible by conduction of ions through the electrolyte. Although the basic principle behind the operation of a fuel cell is quite simple, many challenges have to be overcome before its successful implementation.

The solid oxide fuel cell (SOFC) is one of the types of fuel cells which are of considerable interest since it has considerably high system efficiency in

comparison to other fuel cell systems with cogeneration. The high efficiency of SOFC systems is a result of high operating temperatures and negligible deterioration in performance over several years. The design and handling of complex SOFC systems require efficient control strategies to promote safe and reliable operation. The development of powerful control algorithms is based on an exact knowledge of the operating behaviour, which can be obtained from dynamic system models. The fuel cell system involves multiple energy domains such as chemical, thermal, electrical, hydraulic and mechanical. Furthermore, it involves several phenomena with radically different time scales.

Modelling and applying control theory to such a multidisciplinary system is a challenging task. The bond graph technique is ideally suited for modelling such systems that involve multiple energy domains. Bond graph modelling of SOFC systems ensures that the models are energetically consistent as the conservation laws are built into the bond graph junction structure. Moreover, subsequent modifications to the model can be easily incorporated and the causal structure of the bond graph aids in computer simulation of the system. The simulations are valuable in helping to understand the competing physical processes that are responsible for controlling the cell performance. Such understanding can assist in the cell design and optimisation as well as interpreting the experimental observations. In this chapter, a true bond graph model of the SOFC is presented [12, 13, 15]. This model represents the couplings between the various energy domains in a unified manner and captures all the essential dynamics of the SOFC. The chapter is organised in the following fashion. The description of the SOFC process is given followed by which the important assumptions involved in the modelling are explicitly stated. The formulation of the energy-storing C-field and the entropy-generating R-field that are required for constructing the true bond graph model of the SOFC is discussed next followed by which the true bond graph of the SOFC is presented. Finally, the static and dynamic characteristics of the cell, obtained from the simulations, are discussed.

10.2 Bond Graph Model of the SOFC

10.2.1 Process Description and Modelling Approach

The basic components of the SOFC are the anode, the cathode and the electrolyte, as shown in Fig. 10.1. They are together referred to as the membrane electrode assembly (MEA). Fuel (hydrogen) is supplied to the anode side and air is supplied to the cathode side. At the cathode–electrolyte interface, oxygen molecules accept electrons coming from the external circuit to form oxide ions. The solid electrolyte allows only oxide ions to pass through. At the anode–electrolyte interface, hydrogen molecules present in the fuel react with oxide ions to form steam, and electrons get released. As a result of the potential difference set up between anode and cathode

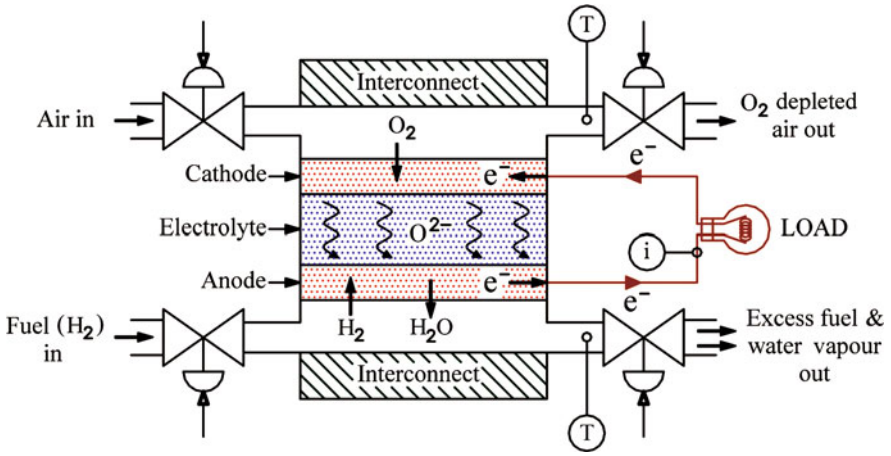

Fig. 10.1 Schematic of an SOFC

due to the resultant excess and scarcity of electrons at anode and cathode, respectively, electric current flows in the external circuit through which they are connected and thus the circuit is closed. Because the reaction is exothermic, heat is evolved as a by-product.

The current drawn from the fuel cell and the temperatures of the anode and cathode channel exhaust gases are the variables that are measured for controlling the valves shown in Fig. 10.1. The pressures in the inlet and the outlet sides are assumed to be known constants and the inlet side temperature is also assumed to be a known constant.

The model presented here is a zero-dimensional bond graph model of a single cell, which is suitable for system dynamics studies and will be helpful in developing control strategies. The cell is considered to be at the centre of the stack such that no edge effects are present. The anode channel volume, through which the supplied hydrogen and the produced water vapour flow, is represented as a single volume and is referred to as the anode channel volume. Similarly the cathode channel volume through which the air flows is represented as a single volume and is referred to as the cathode channel volume. The intensive variables, temperature, pressure and chemical potential, for each gas are assumed to be uniform throughout the control volume. The interconnect plates form the interface between the cells in a stack and also form the channels through which the gases flow. The thermal capacitances of the solids (anode, cathode, electrolyte and interconnect) are lumped. The convective heat transfer taking place between the gases and the MEA and also between the gases and the interconnect plates is modelled. The supply and the removal of gases to and from the channel volumes are through four different controlled valves as shown in Fig. 10.1.

10.2.2 Modelling Assumptions

Some of the important assumptions involved in the modelling are as follows:

1. The water formed due to the reaction is in the vapour form. All the gases involved are assumed to be ideal. This assumption is valid because of the low pressure and high operating temperatures.
2. The fuel considered in this model is pure hydrogen. The oxidant is air with oxygen and nitrogen as its primary constituents.
3. As the cell is well insulated, the heat loss to the surrounding is neglected.
4. As the fast dynamics are irrelevant from control perspective, the diffusion process is modelled through an approximation.

10.2.3 Storage of a Two-Species Gas Mixture

The SOFC channels on the anode side contain the hydrogen and water vapour, while the cathode side has nitrogen and oxygen. On the anode side hydrogen is consumed in the electrochemical reaction and the water vapour is produced, while on the cathode side oxygen is consumed. The nitrogen on the cathode side does not participate in the reaction. A storage element capable of representing the energy storage in a two-species gas mixture is necessary for modelling this scenario. Such a C-field representation is presented in [12, 13, 15]. This is an extension of the C-field representing a single gas species presented in [4, 6, 8]. In this section, the constitutive relations for a bond graph C-field representing the energy storage by two species of gases in a control volume are derived. The two gas species are represented by subscripts 1 and 2. The C-field for the two-species gas mixture proposed here models the following scenario. A mixture of two gases is contained in a collapsible chamber, which allows heat transfer from and to the surroundings. In the general scenario modelled here, it is assumed that individual gases can independently flow either into or out of the chamber. Allowing the individual gas mass flow rates in proportion to their mass fractions in the mixture can also incorporate the mass flow of the mixture as a whole. Although the constitutive relations are given by considering a mixture of two gas species, it can be extended for a mixture of any number of gas species.

The change of internal energy of the two gases in the mixture in terms of time derivatives is given by

$$\dot{U} = \frac{\partial U}{\partial V}\dot{V} + \frac{\partial U}{\partial S}\dot{S} + \frac{\partial U}{\partial m_1}\dot{m}_1 + \frac{\partial U}{\partial m_2}\dot{m}_2 \tag{10.1}$$

From well-known thermodynamic relations, $\partial U/\partial V = -p$, $\partial U/\partial S = T$, $\partial U/\partial m_1 = \mu_1$ and $\partial U/\partial m_2 = \mu_2$, it is evident that the internal energy of the volume of the gases changes due to four distinct power exchanges which can be represented by the products of the corresponding effort and flow variables.

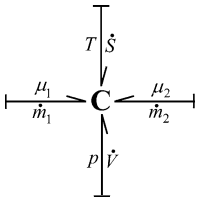

Fig. 10.2 Two species of gases represented in a C-field

Therefore, the energy storage in the gas mixture can be represented as a four-port C-field as shown in Fig. 10.2. This C-field has four power ports: the flow and effort variables for the mechanical port are $\dot{V}$ and p, respectively; those for the thermal port are $\dot{S}$ and T, respectively; and those for the material ports are $\dot{m}$'s and μ's, respectively.

According to the fundamental thermodynamic relation [18], the change in the specific entropy of an ideal gas (gas species #1) in terms of the specific internal energy, the specific volume, the partial pressure and the equilibrium temperature is given by

$$\mathrm{d}s_1 = \frac{\mathrm{d}u_1}{T} + \frac{p_1 \mathrm{d}v_1}{T} \tag{10.2}$$

Using the ideal gas equation of state ($pv = RT$) and the definition of specific heat capacity at constant volume ($\mathrm{d}u = c_\mathrm{v}\mathrm{d}T$), (10.2) may be rewritten as

$$\mathrm{d}s_1 = \frac{c_{\mathrm{v}1}\mathrm{d}T}{T} + \frac{R_1 \mathrm{d}v_1}{v_1} \tag{10.3}$$

Integrating (10.3) from an initial state (indicated by superscript 0) to a final state with the assumption of constant specific heat capacities and then writing the specific quantities in terms of the absolute quantities gives

$$s_1 = \frac{S_1^0}{m_1^0} + \ln\left\{\left(\frac{T}{T^0}\right)^{c_{\mathrm{v}1}}\left(\frac{Vm_1^0}{V^0 m_1}\right)^{R_1}\right\} \tag{10.4}$$

Similarly, for gas species #2, which occupies the same volume and is at the same temperature, we obtain

$$s_2 = \frac{S_2^0}{m_2^0} + \ln\left\{\left(\frac{T}{T^0}\right)^{c_{\mathrm{v}2}}\left(\frac{Vm_2^0}{V^0 m_2}\right)^{R_2}\right\} \tag{10.5}$$

Multiplying (10.4) with m_1 and (10.5) with m_2, we get the following expressions for the entropies of the gas species #1 and #2:

$$S_1 - \frac{S_1^0 m_1}{m_1^0} = \ln\left\{\left(\frac{T}{T^0}\right)^{m_1 c_{v1}}\left(\frac{V m_1^0}{V^0 m_1}\right)^{m_1 R_1}\right\} \tag{10.6}$$

and

$$S_2 - \frac{S_2^0 m_2}{m_2^0} = \ln\left\{\left(\frac{T}{T^0}\right)^{m_2 c_{v2}}\left(\frac{V m_2^0}{V^0 m_2}\right)^{m_2 R_2}\right\} \tag{10.7}$$

The total entropy of a mixture of gases is given by the sum of the entropies of the individual gases:

$$S - \frac{S_1^0 m_1}{m_1^0} - \frac{S_2^0 m_2}{m_2^0} = \ln\left\{\begin{array}{l}\left(\frac{V}{V^0}\right)^{m_1 R_1 + m_2 R_2}\left(\frac{m_1^0}{m_1}\right)^{m_1 R_1} \\ \left(\frac{T}{T^0}\right)^{m_1 c_{v1} + m_2 c_{v2}}\left(\frac{m_2^0}{m_2}\right)^{m_2 R_2}\end{array}\right\} \tag{10.8}$$

where $S = (S_1 + S_2)$.

From (10.8), the temperature of the gases is given as a function of the four state variables (m_1, m_2, V and S):

$$T = T^0 \exp\left(\frac{S}{m_1 c_{v1} + m_2 c_{v2}} - \frac{m_1 S_1^0}{m_1 m_1^0 c_{v1} + m_1^0 m_2 c_{v2}} - \frac{m_2 S_2^0}{m_1 m_2^0 c_{v1} + m_2^0 m_2 c_{v2}}\right)$$
$$\times \left(\frac{V}{V^0}\right)^{-(\alpha_1+\alpha_2)}\left(\frac{m_1}{m_1^0}\right)^{\alpha_1}\left(\frac{m_2}{m_2^0}\right)^{\alpha_2} \tag{10.9}$$

where $\alpha_1 = m_1 R_1/(m_1 c_{v1} + m_2 c_{v2})$ and $\alpha_2 = m_1 R_1/(m_1 c_{v1} + m_2 c_{v2})$. The internal energy of the gas mixture is obtained as the sum of the internal energies of both the gases in the chamber, i.e. $U = m_1 c_{v1} T + m_2 c_{v2} T$, or

$$U = (m_1 c_{v1} + m_2 c_{v2})\, T^0 \left(\frac{V}{V^0}\right)^{-(\alpha_1+\alpha_2)}\left(\frac{m_1}{m_1^0}\right)^{\alpha_1}\left(\frac{m_2}{m_2^0}\right)^{\alpha_2} \tag{10.10}$$
$$\times \exp\left(\frac{S}{m_1 c_{v1} + m_2 c_{v2}} - \frac{m_1 S_1^0}{m_1 m_1^0 c_{v1} + m_1^0 m_2 c_{v2}} - \frac{m_2 S_2^0}{m_1 m_2^0 c_{v1} + m_2^0 m_2 c_{v2}}\right)$$

The total pressure in the chamber is then obtained by summing the partial pressures, i.e. $p = m_1 R_1 T/V + m_2 R_2 T/V$, where T is given by (10.9). The same result can also be obtained by taking the partial derivative of the total internal energy in (10.10) with respect to the total volume:

$$p = T^0 \left(\frac{m_1 R_1 + m_2 R_2}{V} \right) \times \exp \left(\frac{S}{m_1 c_{v1} + m_2 c_{v2}} - \frac{m_1 S_1^0}{m_1 m_1^0 c_{v1} + m_1^0 m_2 c_{v2}} - \frac{m_2 S_2^0}{m_1 m_2^0 c_{v1} + m_2^0 m_2 c_{v2}} \right) \times \left(\frac{V}{V^0} \right)^{-(\alpha_1 + \alpha_2)} \left(\frac{m_1}{m_1^0} \right)^{\alpha_1} \left(\frac{m_2}{m_2^0} \right)^{\alpha_2} \tag{10.11}$$

Likewise, the chemical potentials of the gases can be obtained by taking the partial derivative of U with respect to their corresponding masses. That leads to a cumbersome formula. Alternatively, the chemical potential of gas #1 can be given as

$$\mu_1 = u_1 + p_1 v_1 - T s_1 = c_{v1} T + R_1 T - T s_1 \tag{10.12}$$

Equation (10.12) can be written as

$$\mu_1 = h_1 - T s_1 \tag{10.13}$$

Substituting $h_1 = h_1^0 + \int c_p \mathrm{d}T$ and $s_1 = s_1^0 + \int \left(c_p / T \right) \mathrm{d}T - R_1 \ln \left(p_1 / p_1^0 \right)$ in (10.13), we get

$$\mu_1 = \mu_1^0 (T) + R_1 T \ln \left(\frac{p_1}{p_1^0} \right) \tag{10.14}$$

where $\mu_1^0 (T)$ is purely a function of the temperature. The partial pressure of the gas species #1 and the temperature of the mixture in (10.14) are written in terms of the state variables by using the earlier expressions (refer to (10.9) and (10.11)). The chemical potential of gas #2 is obtained in a similar fashion as

$$\mu_2 = \mu_2^0 (T) + R_2 T \ln \left(\frac{p_2}{p_2^0} \right) \tag{10.15}$$

Equations (10.9), (10.11), (10.14) and (10.15) are the constitutive relations of the four-port C-field as they give the effort variables (μ_1, μ_2, p and T) in terms of the four state variables (m_1, m_2, V and S), which are obtained by integrating the flow variables in the bonds of the four-port C-field.

10.2.4 An Entropy-Generating R-field to Represent the Convection of a Gas Mixture

In this section, an R-field formulation for representing the convection of a two-gas mixture is given [12, 13, 15]. This is an extension of the bond graph formulation for the forced convection of a compressible ideal gas given in [6]. The details of the sub-model for modelling the convection of a two-component gas mixture are given in Fig. 10.3. The most important element in the expanded model of the MR element is the RS-field element (see Fig. 10.3). This element receives the downstream side temperature and the information of the valve position (x), the upstream side chemical potentials and temperature, and the downstream side chemical potentials to calculate the mass and entropy flow rates. Note that all these variables are inputs to the MR element. To maintain the clarity of the figure, the connections needed to explicitly show these modulations are not drawn.

From the causal analysis, this sub-model receives six effort variables and computes six flow variables without the use of integration and/or differentiation. Therefore, this sub-model can be represented as an encapsulated R-field (a six-port element MR in Fig. 10.3). From the continuity equation, the mass flow rate of a particular gas is the same for the inlet and the outlet side. This reduces the total number of independent flow variables to four (see Fig. 10.3). Then the constitutive relation of the non-linear resistive field element is given as

$$\left(\dot{S}_\mathrm{u}, \dot{S}_\mathrm{d}, \dot{m}_1, \dot{m}_2\right)^\mathrm{T} = \Phi_\mathrm{R}\left\{\left(T_\mathrm{u}, T_\mathrm{d}, \mu_{1\mathrm{u}}, \mu_{1\mathrm{d}}, \mu_{2\mathrm{u}}, \mu_{2\mathrm{d}}\right)^\mathrm{T}\right\} \tag{10.16}$$

where, Φ_R is a vector-valued function. The individual relations between the input and the output variables are derived as follows.

The overall mass flow rate ($\dot{m}$) of the mixture is imposed at the $1_{\dot{m}}$ junction by the modulated RS-field element in Fig. 10.3 and it is given by the linear nozzle equation:

$$\dot{m} = K\left(p_\mathrm{u} - p_\mathrm{d}\right) \tag{10.17}$$

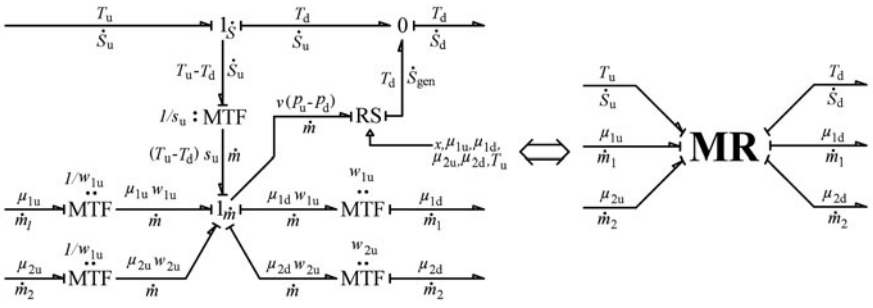

Fig. 10.3 Bond graph representation for convection of a two-component gas mixture

Note that although the total upstream and downstream side pressures are needed in (10.17), they can indeed be calculated from the chemical potentials and temperatures. These calculations are given later in this section (see (10.24) and (10.25)). The individual mass flow rates of the two gases are then realised through the modulated transformer elements shown in Fig. 10.3 as $\dot{m}_1 = \dot{m} w_{1u}$ and $\dot{m}_2 = \dot{m} w_{2u}$. The upstream mass fractions w_{1u} and w_{2u} are obtained from the upstream side storage element, i.e. $w_{1u} = m_{1u}/(m_{1u} + m_{2u})$, $w_{2u} = m_{2u}/(m_{1u} + m_{2u})$ and $w_{1u} + w_{2u} = 1$, where m_{1u} and m_{2u} are the contemporary masses (state variables) in the upstream side control volume.

The entropy flow rate associated with the mass flow rate is calculated by means of a transformer element (between junctions $1_{\dot{S}}$ and $1_{\dot{m}}$), which is modulated by the specific entropy of the upstream side gases. This information of the upstream side specific entropy either can be obtained directly from the upstream side storage element or, if a standalone scheme is required, can be calculated from the upstream side μ's and T's (which are inputs of the MR element) as

$$s_u = c_{p1} w_{1u} + c_{p2} w_{2u} - \frac{(\mu_{1u} w_{1u} + \mu_{2u} w_{2u})}{T_u} \tag{10.18}$$

The entropy flow rate from the upstream side is given as $\dot{S}_u = \dot{m} s_u$. The R-field represents the change in the intensive variables between the upstream and the downstream sides. The temperatures, pressures and the chemical potentials of the gas mixture in the upstream and the downstream sides are imposed by the storage elements on the corresponding sides. Due to this, there is an enthalpy difference between the upstream and the downstream sides, which can be represented as the relation between the changes in the intensive variables by using the Gibbs–Duhem equation [5] as

$$v\,(p_u - p_d) = s_u\,(T_u - T_d) + w_{1u}\,(\mu_{1u} - \mu_{1d}) + w_{2u}\,(\mu_{2u} - \mu_{2d}) \tag{10.19}$$

This relation is enforced by the $1_{\dot{m}}$ junction in Fig. 10.3. Due to the enthalpy difference between the upstream and the downstream side gases, entropy is generated in the resistive field. Using the principle of power conservation, the irreversible entropy generated $\dot{S}_{gen}$ can be given as

$$\dot{S}_{gen} = \frac{\dot{m} v\,(P_u - P_d)}{T_d} \tag{10.20}$$

Substitution of (10.20) into (10.19) gives

$$\dot{S}_{gen} = \frac{\dot{m}\,(s_u\,(T_u - T_d) + w_{1u}\,(\mu_{1u} - \mu_{1d}) + w_{2u}\,(\mu_{2u} - \mu_{2d}))}{T_d} \tag{10.21}$$

where $s_u\,(T_u - T_d) + w_{1u}\,(\mu_{1u} - \mu_{1d}) + w_{2u}\,(\mu_{2u} - \mu_{2d})$ and T_d are effort inputs to the RS-element and $\dot{m}$ is calculated internally from the constitutive relation of the

RS-element (see (10.17)). The downstream side entropy flow rate is the sum of the upstream side entropy flow rate ($\dot{S}_u$ imposed at $1_{\dot{S}}$ junction by the MTF element) and the irreversible entropy generated ($\dot{S}_{gen}$ in (10.21)). This sum is realised by means of the zero junction shown in Fig. 10.3.

The upstream and downstream pressures, which are needed in (10.17), can either be read directly from the upstream and downstream side storage elements or be calculated as functions of μ's and T's (the input variables to the MR element) as follows. The change in the upstream side specific entropy of a given mass of gas species #1 is given by

$$s_{1u} - s_{1u}^0 = \ln\left(\left(\frac{T_u}{T_u^0}\right)^{c_{v1}}\left(\frac{v_{u1}}{v_{u1}^0}\right)^{R_1}\right) \tag{10.22}$$

Substitution of $s_{1u} = C_{p1} - \mu_{1u}/T_u$ in (10.22) and rearrangement gives

$$v_{u1} = v_{u1}^0 \exp\left(-\frac{\mu_{1u}}{T_u R_1} + \frac{\mu_{1u}^0}{T_u^0 R_1}\right)\left(\frac{T_u}{T_u^0}\right)^{-\frac{c_{v1}}{R_1}} \tag{10.23}$$

The upstream side partial pressure of gas species #1 is given as

$$p_{1u} = \frac{R_1 T_u}{v_{u1}} = p_{u1}^0 \exp\left(\frac{\mu_{1u}}{T_u R_1} - \frac{\mu_{1u}^0}{T_u^0 R_1}\right)\left(\frac{T_u}{T_u^0}\right)^{\frac{c_{v1}}{R_1}} \tag{10.24}$$

Similarly, the upstream partial pressure of gas #2 is

$$p_{2u} = \frac{R_2 T_u}{v_{u2}} = p_{u2}^0 \exp\left(\frac{\mu_{2u}}{T_u R_2} - \frac{\mu_{2u}^0}{T_u^0 R_2}\right)\left(\frac{T_u}{T_u^0}\right)^{\frac{c_{v2}}{R_2}} \tag{10.25}$$

The total upstream side pressure is $p_u = p_{1u} + p_{2u}$. The total downstream side pressure can also be expressed similarly.

10.2.5 True Bond Graph Model of the SOFC

The true bond graph model of the SOFC system is given in Fig. 10.4. This model uses the four-port C-field (presented in Section 10.2.3) for representing the energy storage of the gases inside the anode and the cathode flow channels. It also uses the R-field representation discussed in Section 10.2.4 for modelling the convection at the inlet and the outlet of the SOFC channels.

Representing a thermodynamic system in terms of true bond graph involves the concepts of network thermodynamics [9]. The true bond graph model of the SOFC, shown in Fig. 10.4, is constructed by using the concepts of network

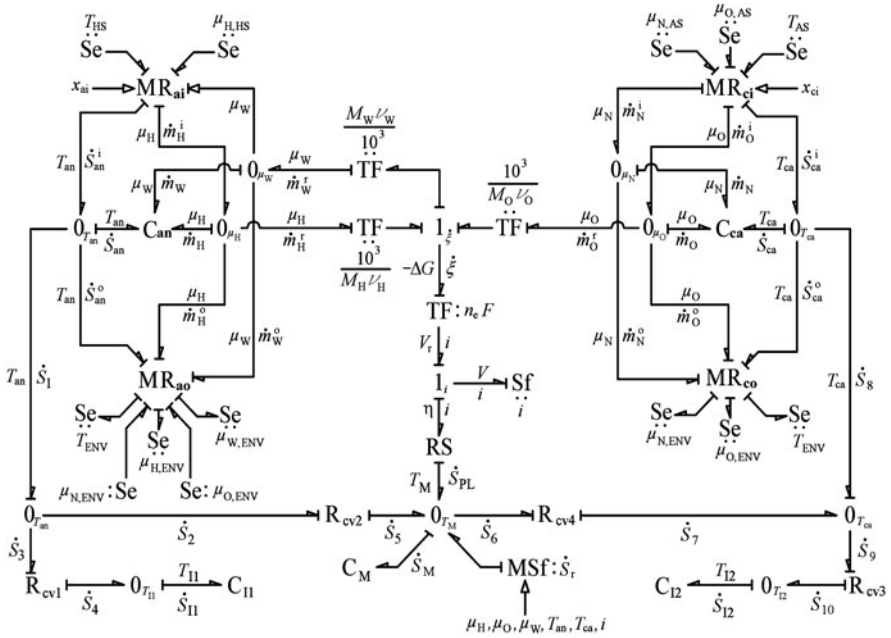

Fig. 10.4 True bond graph model of the SOFC

thermodynamics. As the volumes of both the channels remain constant, the mechanical ports of the C-fields are not shown in Fig. 10.4. The mass and entropy balances of the anode and cathode channel control volumes are given by the corresponding zero junctions in Fig. 10.4. The $0_{T_{an}}$ and the $0_{T_{ca}}$ junctions give the entropy balances for the anode channel and the cathode channel control volumes, respectively. The 0_{μ_H}, 0_{μ_W}, 0_{μ_O} and 0_{μ_N} junctions give the mass balances for the hydrogen, water vapour, oxygen and nitrogen gases, respectively, in the control volumes. The 0_{T_M} junction gives the entropy balance at the MEA solid control volume.

The capacitive elements and fields in the model represent equilibrium thermodynamics part of the model. As the simulation proceeds, the matter inside the control volume represented by these elements changes reversibly from one equilibrium state to the next, i.e. the process is assumed to be quasi-static. The R-fields represent the non-equilibrium parts of the model, and they introduce the irreversibilities into the system. The R-field elements represented by 'MR' in Fig. 10.4 introduce the irreversibility due to mass convection into the system (refer to Section 10.2.4). The R-field element represented by 'RS' in Fig. 10.4 introduces the irreversibility due to the over-voltage phenomena (ohmic, concentration and activation losses). The other R-field elements introduce the irreversibilities due to the heat transfer phenomena.

The inlet and outlet valve resistances are modelled by the MR-fields described in Section 10.2.4, where subscripts mentioned in the nomenclature identify them. The valve resistances in the MR-fields may be controlled by modifying the variables for the stem positions. Note that although only hydrogen gas flows through the anode

side inlet valve, the information of chemical potential of water vapour (μ_W) inside the anode channel is required for computing the downstream side pressure, which is supplied by an information bond in Fig. 10.4. Similarly, the additional information of the chemical potentials of nitrogen and oxygen in the atmosphere is required in the anode channel outlet valve model to calculate the downstream side pressure, which is provided by the source of efforts as shown in Fig. 10.4. The downstream side entropy flow is the sum of the upstream side entropy flow and the entropy generated due to the enthalpy difference between the upstream and the downstream sides (10.21).

In this model, the chemical potentials of the gases not only drive the electrochemical reaction but also, along with temperatures, determine the flow of the gases in and out of the channels. This is because, though the mass flow through the MR-field element is determined from the upstream and downstream side pressures (10.17), the individual pressures can be written as functions of the chemical potential and the temperature ((10.24) and (10.25)). Thus, the coupling between the chemical, thermal, mechanical and the hydraulic domains, which is encountered in a fuel cell system, is effectively represented in a unified manner by using true bond graphs.

The transformation of power from the chemical domain into the electrical domain is implemented by the 1_ξ junction and the transformers surrounding it as shown in Fig. 10.4. This transformation is discussed in the following. The change in the Gibbs free energy of the system is given as

$$\mathrm{d}G = V\mathrm{d}p - S\mathrm{d}T + \mu\mathrm{d}m \tag{10.26}$$

Using (10.26) and the assumption of constant temperature and pressure, the change in the Gibbs free energy of the reaction is obtained as

$$\mathrm{d}G = \frac{\partial G}{\partial n_W}\mathrm{d}n_W - \frac{\partial G}{\partial n_H}\mathrm{d}n_H - \frac{\partial G}{\partial n_O}\mathrm{d}n_O \tag{10.27}$$

Note that the temperature and the pressure of the system may change during the system's dynamics. However, (10.27) is assumed to be valid for each instantaneous values of pressure and temperature of the system. A quantity called the reaction coordinate (ξ) is defined such that $\mathrm{d}n_H = -\nu_H\mathrm{d}\xi$, $\mathrm{d}n_O = -\nu_O\mathrm{d}\xi$ and $\mathrm{d}n_W = \nu_W\mathrm{d}\xi$. Using these relations and the definition of the chemical potential, (10.27) becomes

$$\mathrm{d}G = (\mu_W\nu_W - \mu_H\nu_H - \mu_O\nu_O)\,\mathrm{d}\xi \tag{10.28}$$

As the quantities in (10.28) are state functions, the equation can be written as

$$\Delta G = (\mu_W\nu_W - \mu_H\nu_H - \mu_O\nu_O)\,\Delta\xi \tag{10.29}$$

If unit mole of fuel (hydrogen) is considered then $\Delta\xi = 1$. Therefore, the change in the Gibbs free energy per mole of fuel is given by

$$\Delta G = \mu_{\mathrm{W}} \nu_{\mathrm{W}} - \mu_{\mathrm{H}} \nu_{\mathrm{H}} - \mu_{\mathrm{O}} \nu_{\mathrm{O}} \tag{10.30}$$

Note that the chemical potentials are in J mol^{-1} in (10.30). Under reversible conditions, this change in the Gibbs free energy is converted entirely into electrical energy. Therefore, from the energy balance, the reversible cell voltage can be obtained as

$$V_{\mathrm{r}} = -\frac{\Delta G}{n_{\mathrm{e}} F} \tag{10.31}$$

where the denominator gives the charge of the total number of electrons participating in the reaction per mole of the fuel. Equation (10.31) can further be written in terms of the partial pressures of the reactant and the product gases and is called the Nernst equation. The Nernst equation is used to calculate the effect of the change in the partial pressures of the reacting species on the reversible cell voltage. Note that the minus sign in (10.31) is required to obtain a positive value of voltage because the change in the Gibbs free energy per mole as defined in (10.30) is negative (as the free energy of the products is less than the free energy of the reactants).

The chemical potentials are calculated in J kg^{-1} in the anode and cathode channel C-fields of the model. The three transformers shown in the effort-activated bonds around the $1_{\dot{\xi}}$ junction have factors of '$1000/M_i$' in order to convert the chemical potentials to J mol^{-1}. The $1_{\dot{\xi}}$ junction shown in Fig. 10.4 enforces the following relationship, which defines the negative of the change in Gibbs free energy per mole of fuel for the reaction:

$$-\Delta G = \frac{\nu_{\mathrm{H}} M_{\mathrm{H}} \mu_{\mathrm{H}} + \nu_{\mathrm{O}} M_{\mathrm{O}} \mu_{\mathrm{O}} - \nu_{\mathrm{W}} M_{\mathrm{W}} \mu_{\mathrm{W}}}{1000} \tag{10.32}$$

The reversible cell voltage, which is defined by the Nernst equation, is realised by means of a transformer element (with modulus $n_{\mathrm{e}} F$) in Fig. 10.4. When the reaction system is in equilibrium, the change in the molar Gibbs free energy (ΔG) is zero. Therefore, the reversible voltage as predicted by the Nernst equation is also zero. When the reaction system is forced out of equilibrium (i.e. when the concentrations of the reactants and the products differ from the equilibrium concentrations), the reversible open-circuit voltage (V_{r}) can be calculated by using the Nernst equation. However, the reaction cannot proceed as the circuit is not closed. But once the circuit is closed (as we try to draw current from the cell), the irreversibilities come into play and result in voltage losses.

The mole flow rate of the reaction ($\dot{\xi}$), which can be considered as the reaction rate, is related to the mole flow rates of consumption and production of the reactants and products, respectively, as

$$\dot{\xi} = \frac{\dot{n}^{\mathrm{r}}_{\mathrm{W}}}{\nu_{\mathrm{W}}} = -\frac{\dot{n}^{\mathrm{r}}_{\mathrm{H}}}{\nu_{\mathrm{H}}} = -\frac{\dot{n}^{\mathrm{r}}_{\mathrm{O}}}{\nu_{\mathrm{O}}} \tag{10.33}$$

The reaction mole flow rate and the current (i) are related as

$$i = \dot{\xi} n_e F \tag{10.34}$$

Therefore, the relations between the mass flow rates (in kg s^{-1}) of hydrogen, oxygen and water vapour taking part in the reaction and the current drawn by the load are given as

$$i = \frac{1000 n_e F \dot{m}^r_W}{\nu_W M_W} = -\frac{1000 n_e F \dot{m}^r_H}{\nu_H M_H} = -\frac{1000 n_e F \dot{m}^r_O}{\nu_O M_O} \tag{10.35}$$

and they are realised through the $1_{\dot{\xi}}$ junction and the set of transformers in the flow-activated bonds surrounding it as shown in Fig. 10.4. The current, i, drawn by an un-modelled external load is represented by a source of flow.

The theoretical open-circuit voltage (V_r) is the maximum voltage that can be achieved by a fuel cell under specific operating conditions. However, the voltage of an operating cell, which is equal to the voltage difference between the cathode and the anode, is generally lower than this. As current is drawn from a fuel cell, the cell voltage falls due to the internal resistances and over-voltage losses. The electrode over-voltage losses are associated with the electrochemical reactions taking place at the electrode/electrolyte interfaces and can be divided into concentration and activation over-voltages. The actual cell voltage is generally obtained by subtracting all the voltage losses from the open-circuit voltage.

Three different kinds of voltage losses or over-voltages contribute to the cell irreversibility. Activation over-voltage refers to the over-potential required to exceed the activation energy barrier so that the electrode reactions proceed at the desired rate [17]. The anodic and the cathodic activation over-voltages are governed by the Butler–Volmer equation [3] which in its general form is given as

$$i = i_0 \left\{ \exp\left(\frac{\beta n_e F \eta_{act}}{RT} \right) - \exp\left(\frac{-(1-\beta) n_e F \eta_{act}}{RT} \right) \right\} \tag{10.36}$$

If the transfer coefficient (β) is 0.5, which is normally the case, the anodic and cathodic activation over-voltages can be obtained from (10.36) as

$$\eta_{act,an} = \frac{2RT_M}{n_e F} \sinh^{-1}\left(\frac{0.5i}{i_{0,an}} \right) \tag{10.37}$$

and

$$\eta_{act,ca} = \frac{2RT_M}{n_e F} \sinh^{-1}\left(\frac{0.5i}{i_{0,c}} \right) \tag{10.38}$$

where the anodic and the cathodic exchange currents are given as

$$i_{0,\mathrm{an}} = \psi_{\mathrm{an}} A_{\mathrm{c}} \left(\frac{p_{\mathrm{H}}}{p_{\mathrm{amb}}}\right)\left(\frac{p_{\mathrm{W}}}{p_{\mathrm{amb}}}\right) \exp\left(\frac{-E_{\mathrm{an}}}{RT_{\mathrm{M}}}\right)$$

and

$$i_{0,\mathrm{ca}} = \psi_{\mathrm{ca}} A_{\mathrm{c}} \left(\frac{p_{\mathrm{O}}}{p_{\mathrm{amb}}}\right)^{0.25} \exp\left(\frac{-E_{\mathrm{ca}}}{RT_{\mathrm{M}}}\right)$$

It is clear from (10.37) and (10.38) that the contribution of the activation over-voltage to the overall voltage loss is significant at low currents. The ohmic over-voltage (η_{ohm}) is due to the resistance to the transport of ions in the electrolyte and to the flow of electrons through the electrodes and current collectors. It is governed by Ohm's law:

$$\eta_{\mathrm{ohm}} = iR_{\mathrm{ohm}} \tag{10.39}$$

where R_{ohm} is the resistance per unit area. The ohmic over-voltage comes into play typically at the middle range of current densities within which the fuel cell is usually designed to operate. However, due to load fluctuations during operation, the fuel cell may have to be operated at low and high current density conditions, where other kinds of over-voltages are predominant.

The reactants, i.e. hydrogen and oxygen, in the flow channels have to diffuse through the porous anode and cathode, respectively, to reach the electrode–electrolyte interface where the reaction occurs. Similarly, the product of the reaction, i.e. water vapour, which is formed at the anode–electrolyte interface, has to diffuse through the porous anode so as to reach the flow bulk in the anode channel. If the cell is functioning reversibly, the partial pressures of the reactant and the product gas species are same at the flow bulk in the gas channels and at the triple phase boundary (TPB) where the actual reaction takes place (called so because of the presence of three phases, viz. the solid nickel or lanthanum strontium manganite of the electrodes, the solid yttria-stabilised zirconium oxide phase of the ceramic electrolyte and the gas phase of either the reactants or the products). But when current is drawn from the cell, the partial pressures of the gas species at the TPB differ from their corresponding partial pressures in the bulk due to limitations imposed by the diffusion process (refer to Fig. 10.5). The voltage lost due to this pressure difference between the bulk and the TPB is called as the concentration over-voltage.

By assuming that the pressure loss of one of the reactants, say hydrogen, determines the concentration over-voltage and that the pressure drop between the bulk and the TPB region is linear, a simple expression for the concentration over-voltage can be derived as follows. If the system is at steady state, then the absolute rate of diffusion of the gas for a unit of geometric area must be equal to the current. Therefore

$$i = k(p_{\mathrm{H,b}} - p_{\mathrm{H,TPB}}) \tag{10.40}$$

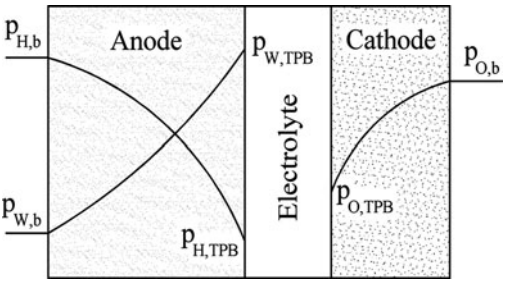

Fig. 10.5 Schematic showing the variation of the partial pressures of hydrogen and water vapour through the anode and oxygen through the cathode

Moreover, $p_{\mathrm{H,TPB}}$ tends to zero as the current 'i' tends to a limiting value 'i_{L}'. So we can write

$$p_{\mathrm{H,b}} = \frac{i_{\mathrm{L}}}{k} \tag{10.41}$$

Substituting (10.41) into (10.40), we get

$$p_{\mathrm{H,TPB}} = \frac{(i_{\mathrm{L}} - i)}{k} \tag{10.42}$$

The difference in the Nernst voltages calculated by using the partial pressures of the reacting gas species at the bulk and the TPB gives the concentration over-voltage. The reversible Nernst voltage of the cell is represented in terms of the species partial pressures and temperature as

$$V_{\mathrm{r}} = -\frac{\Delta G^0}{n_{\mathrm{e}} F} - \mathrm{R}T \ln\left(\frac{p_{\mathrm{W}}^{\nu_{\mathrm{W}}}}{p_{\mathrm{H}}^{\nu_{\mathrm{H}}} p_{\mathrm{O}}^{\nu_{\mathrm{O}}}}\right) \tag{10.43}$$

where $\Delta G^0 = \mu_{\mathrm{W}}^0 \nu_{\mathrm{W}} - \mu_{\mathrm{H}}^0 \nu_{\mathrm{H}} - \mu_{\mathrm{O}}^0 \nu_{\mathrm{O}}$, which is the change in the Gibbs free energy of the reaction at the reference state. The concentration over-voltage is obtained by subtracting the Nernst voltage (10.43) obtained by using the partial pressures at the flow bulk and those at the TPB as

$$\eta_{\mathrm{conc}} = -\mathrm{R}T \ln\left(\frac{p_{\mathrm{W,b}}^{\nu_{\mathrm{W}}}}{p_{\mathrm{H,b}}^{\nu_{\mathrm{H}}} p_{\mathrm{O,b}}^{\nu_{\mathrm{O}}}}\right) + \mathrm{R}T \ln\left(\frac{p_{\mathrm{W,TPB}}^{\nu_{\mathrm{W}}}}{p_{\mathrm{H,TPB}}^{\nu_{\mathrm{H}}} p_{\mathrm{O,TPB}}^{\nu_{\mathrm{O}}}}\right) \tag{10.44}$$

It is assumed that the pressure loss of hydrogen alone is significant and is responsible for the concentration over-voltage. Imposing this assumption on (10.44) results in

$$\eta_{\mathrm{conc}} = \frac{RT_{\mathrm{M}}}{n_{\mathrm{e}} F} \ln\left(\frac{p_{\mathrm{H,b}}}{p_{\mathrm{H,TPB}}}\right) \tag{10.45}$$

Substitution of (10.41) and (10.42) into (10.45) yields

$$\eta_{\text{conc}} = \frac{RT_{\text{M}}}{n_{\text{e}}F} \ln\left(\frac{i_{\text{L}}}{i_{\text{L}} - i}\right) = -\frac{RT_{\text{M}}}{n_{\text{e}}F} \ln\left(1 - \frac{i}{i_{\text{L}}}\right) \tag{10.46}$$

The concentration over-voltage is significant only at high currents. From (10.46), it can be understood that the concentration over-voltage is very less when $i << i_{\text{L}}$. It becomes significantly high when the value of the current approaches the limiting current. Note that (10.46) is not valid for $i = i_{\text{L}}$.

All these over-voltages are modelled by the RS-field shown in Fig. 10.4. The effort output (for the port with current as the flow input) of the RS-field is given as

$$\eta = \frac{RT_{\text{M}}}{n_{\text{e}}F}\left(2\sinh^{-1}\left(\frac{0.5i}{i_{0,\text{a}}}\right) + 2\sinh^{-1}\left(\frac{0.5i}{i_{0,\text{c}}}\right) - \ln\left(1 - \frac{i}{i_{\text{L}}}\right)\right) + iR_{\text{ohm}} \tag{10.47}$$

and the flow output (for the port with temperature as the effort input), i.e. the entropy flow rate which goes to the heat transfer part of the model, is given as

$$\dot{S}_{\text{PL}} = \frac{iR}{n_{\text{e}}F}\left(2\sinh^{-1}\left(\frac{0.5i}{i_{0,\text{a}}}\right) + 2\sinh^{-1}\left(\frac{0.5i}{i_{0,\text{c}}}\right) - \ln\left(1 - \frac{i}{i_{\text{L}}}\right)\right) + \frac{i^2 R_{\text{ohm}}}{T_{\text{M}}} \tag{10.48}$$

The $0_{T_{\text{M}}}$ junction shown in Fig. 10.4 represents the temperature of the MEA solid. Convection is an important means of heat transfer in an SOFC as the gases flow through the anode and the cathode channels. Due to the ideal gas assumption and the low velocities, the flow in a fuel cell is usually laminar. The bond graph model shown in Fig. 10.4 includes the convective heat transfers between the anode and cathode channel gases, the MEA and the interconnects. The R-fields, R_{cv2} and R_{cv4}, model the convective heat transfers between the gases and the MEA and the R-fields, R_{cv1} and R_{cv3}, model the convective heat transfers between the gases and the interconnects denoted by I1 and I2, respectively, in Fig. 10.4. The constitutive relations of the R-field, R_{cv1}, are given as [8, 11]

$$\dot{S}_3 = \frac{\lambda_{\text{an}} A_{\text{c}} (T_{\text{I1}} - T_{\text{an}})}{T_{\text{an}}} \tag{10.49}$$

and

$$\dot{S}_4 = \frac{\lambda_{\text{an}} A_{\text{c}} (T_{\text{I1}} - T_{\text{an}})}{T_{\text{I1}}} \tag{10.50}$$

The constitutive relations for the other R-field elements defining the convection heat transfer (R_{cv2}, R_{cv3} and R_{cv4}) are defined in a similar fashion. The thermal capacity of the MEA is represented by the compliance element C_{M} in Fig. 10.4. The constitutive relation of thermal capacity [7, 11] of C_{M} element is given as

$$T_{\mathrm{M}} = T_{\mathrm{M}}^{0} \exp\left(\frac{S_{\mathrm{M}} - S_{\mathrm{M}}^{0}}{m_{\mathrm{M}} c_{\mathrm{M}}}\right) \tag{10.51}$$

The thermal capacitance of the interconnect plates is represented by the two capacitive elements C_{I1} and C_{I2}. The constitutive relation of C_{I1} (that of the other is similar) is given as

$$T_{\mathrm{I1}} = T_{\mathrm{I1}}^{0} \exp\left(\frac{S_{\mathrm{I1}} - S_{\mathrm{I1}}^{0}}{m_{\mathrm{I1}} c_{\mathrm{I1}}}\right) \tag{10.52}$$

The enthalpy of the reaction is given as

$$\Delta H = \Delta G + T\Delta S \tag{10.53}$$

where the part $T\Delta S$ is released as heat when the fuel cell operates reversibly. Under irreversible operation (under all realistic circumstances), the change in the Gibbs free energy of the reaction (ΔG) is not completely converted into useful electrical work. Rather, some of it ends up as heat energy. These irreversibilities, which are called over-voltages, give rise to entropy generation and are taken care of by the RS-field element in the model. In order to account for the entropy change of the reaction, the following entropy flow rate is added to the MEA by means of a modulated source of flow in Fig. 10.4:

$$\dot{S}_{\mathrm{r}} = \frac{\dot{m}_{\mathrm{H}}^{\mathrm{r}}\,(h_{\mathrm{H}} - \mu_{\mathrm{H}})}{T_{\mathrm{an}}} + \frac{\dot{m}_{\mathrm{O}}^{\mathrm{r}}\,(h_{\mathrm{O}} - \mu_{\mathrm{O}})}{T_{\mathrm{ca}}} - \frac{\dot{m}_{\mathrm{W}}^{\mathrm{r}}\,(h_{\mathrm{W}} - \mu_{\mathrm{W}})}{T_{\mathrm{an}}} \tag{10.54}$$

where the specific enthalpies are expressed as follows [2]:

$$h = R\left(a_1 T + a_2 T^2 + a_3 T^3 + a_4 T^4 + a_5 T^5\right) + h_0 \tag{10.55}$$

The values of the coefficients $a_1, \ldots, a_6$ and h_0 for the different gases are taken from [2]. The source of flow MSf:$\dot{S}_{\mathrm{r}}$ is modulated with signals i (to calculate $\dot{m}_{\mathrm{H}}^{\mathrm{r}}$, $\dot{m}_{\mathrm{O}}^{\mathrm{r}}$ and $\dot{m}_{\mathrm{W}}^{\mathrm{r}}$ according to (10.54)), μ_{W}, μ_{H}, μ_{O}, T_{an} and T_{ca} (the later five are calculable from state variables). Note that these modulating signals are not shown in Fig. 10.4 to maintain the visual clarity of the figure.

Unlike the pseudo-bond graphs, the energetic consistency of the true bond graph presented in Fig. 10.4 is apparent. The continuity of energy flows across different domains and across different interfaces is ensured because the effort and the flow variables correspond to the power variables in the corresponding energy domains throughout the bond graph model. All the storage elements in the global model given in Fig. 10.4 are in integral causality. There is no causality violation at any place in the junction structure. This ensures the energy consistency in the model. Moreover, this integrally causalled model does not have algebraic or causal loops, which ensures that this model is well computable.

10.3 Open- and Closed-Loop Dynamic Simulations

10.3.1 Model Initialisation

In this section, the true bond graph model of the SOFC described in Section 10.2.5 is simulated to obtain the static characteristic curves and dynamic responses to a step change in the load current. In order to simulate the steady-state operation of the SOFC, the single port C-elements in the true bond graph model have to be initialised with the values of generalised displacements (initial entropies in this case). Similarly, the two C-field elements have to be initialised with the values of the initial masses of the constituent gases and their entropies.

The fuel utilisation (FU) and oxygen utilisation (OU) are two of the most important control variables of the fuel cell. Fuel utilisation (ζ_f) is defined as the ratio of the mass flow rate of the fuel taking part in the reaction to the mass flow rate of the fuel supplied to the cell. Oxygen utilisation (ζ_o) is defined as the ratio of mass flow rate of oxygen consumed by the reaction to the mass flow rate of oxygen supplied to the cell. According to the operational requirement of the SOFC, FU must be maintained constant. Normally, FU of 0.8–0.9 is desired. In this case, a value of 0.8 is chosen for the FU and a value of 0.125 is chosen for the OU.

For obtaining the static performance curves of the SOFC, the variables such as the operating temperature, the desired current density, the desired total anode and cathode channel pressures (p^0_{an},p^0_{ca}), the FU (ζ_f), the OU (ζ_o), the source and the sink pressures (p_{HS}, p_{AS}, p_{ENV}) and the species mass fractions at the air source ($w_{O,AS}$ and $w_{N,AS}$) are considered as the known variables. We need to establish relationships between the steady-state values of these known variables and the steady-state partial pressures of the individual gas species in the channels so as to obtain the steady-state characteristic curves corresponding to different operating conditions.

In order to establish the desired relations, the steady-state mass balances for the anode and the cathode channels are written. From those mass balance equations, the valve coefficients (which are unknown variables) which will lead to the desired steady-state operation are obtained. In the following discussions, the superscript '0' refers to the desired steady-state value of the variable which needs to be set for obtaining the desired static characteristic curves. The steady-state mass balance in the anode channel by taking into consideration the required value of FU is given as

$$\dot{m}^{i}_{H} = \dot{m}^{r}_{H} + \dot{m}^{o}_{H} \tag{10.56}$$

$$\dot{m}^{r}_{W} = \dot{m}^{o}_{W} \tag{10.57}$$

and

$$\dot{m}^{r}_{H} = \zeta_f \dot{m}^{i}_{H} \tag{10.58}$$

where the hydrogen inlet and outlet mass flow rates and the water vapour outlet mass flow rate are given by the linear nozzle flow equations:

$$\dot{m}_{\mathrm{H}}^{\mathrm{i}} = K_{\mathrm{ai}} \left(p_{\mathrm{HS}} - p_{\mathrm{an}}^{0} \right) \tag{10.59}$$

$$\dot{m}_{\mathrm{H}}^{\mathrm{o}} = K_{\mathrm{ao}} w_{\mathrm{H,an}}^{0} \left(p_{\mathrm{an}}^{0} - p_{\mathrm{ENV}} \right) \tag{10.60}$$

$$\dot{m}_{\mathrm{W}}^{\mathrm{o}} = K_{\mathrm{ao}} w_{\mathrm{W,an}}^{0} \left(p_{\mathrm{an}}^{0} - p_{\mathrm{ENV}} \right) \tag{10.61}$$

Note that in (10.56), (10.57), (10.58), (10.59), (10.60) and (10.61), the unknown variables are K_{ai}, K_{ao}, $w_{\mathrm{H,an}}^{0}$ and $w_{\mathrm{W,an}}^{0}$. However, the total steady-state mass in the anode channel can be calculated using the ideal gas law because the desired anode channel pressure, temperature and the volume are known. Therefore, the three equations (10.56), (10.57) and (10.58) are solved for the two valve coefficients (K_{ai} and K_{ao}) and for the ratio of the mass fractions, i.e.

$$\frac{w_{\mathrm{W,an}}^{0}}{w_{\mathrm{H,an}}^{0}} = \frac{m_{\mathrm{W,an}}^{0}}{m_{\mathrm{H,an}}^{0}} = \frac{n_{\mathrm{W,an}}^{0} M_{\mathrm{W}}}{n_{\mathrm{H,an}}^{0} M_{\mathrm{H}}} \tag{10.62}$$

Solving (10.56), (10.57) and (10.58), we get the expressions for the inlet and outlet valve coefficients as

$$K_{\mathrm{ai}} = \frac{\dot{m}_{\mathrm{H}}^{\mathrm{r}}}{\zeta_{\mathrm{f}} p_{\mathrm{HS}} - \zeta_{\mathrm{f}} p_{\mathrm{an}}^{0}} \tag{10.63}$$

and

$$K_{\mathrm{ao}} = \frac{\dot{m}_{\mathrm{W}}^{\mathrm{r}}}{w_{\mathrm{W,an}}^{0} p_{\mathrm{an}}^{0} - w_{\mathrm{W,an}}^{0} p_{\mathrm{ENV}}} \tag{10.64}$$

and the ratio of the partial pressures of the two gas species in the anode channel is found to be

$$\frac{n_{\mathrm{H,an}}^{0}}{n_{\mathrm{W,an}}^{0}} = \frac{p_{\mathrm{H}}^{0}}{p_{\mathrm{W}}^{0}} = \frac{1 - \zeta_{\mathrm{f}}}{\zeta_{\mathrm{f}}} \tag{10.65}$$

As we know the total pressure in the anode channel, we can calculate the individual partial pressures of hydrogen and water vapour, thus establishing the relationship between the FU and the partial pressures of individual species.

Similarly, the mass balance equations for the cathode channel volume result in the expressions for the cathode channel inlet and outlet valve coefficients as

$$K_{\mathrm{ci}} = \frac{\dot{m}_{\mathrm{O}}^{\mathrm{r}}}{\zeta_{\mathrm{o}} \left(w_{\mathrm{O,AS}} p_{\mathrm{AS}} - w_{\mathrm{O,AS}} p_{\mathrm{ca}}^{0} \right)} \tag{10.66}$$

and

$$K_{\mathrm{ci}} = \frac{\dot{m}_{\mathrm{O}}^{\mathrm{r}}}{\zeta_{\mathrm{o}} \left(w_{\mathrm{O,AS}} p_{\mathrm{AS}} - w_{\mathrm{O,AS}} p_{\mathrm{ca}}^{0} \right)} \tag{10.67}$$

and also the ratio of the partial pressures of the two gas species as

$$\frac{n_{\mathrm{N,AS}}^{0}}{n_{\mathrm{O,AS}}^{0} \left(1 - \zeta_{\mathrm{o}}\right)} = \frac{n_{\mathrm{N,ca}}^{0}}{n_{\mathrm{O,ca}}^{0}} = \frac{p_{\mathrm{N}}^{0}}{p_{\mathrm{O}}^{0}} \tag{10.68}$$

By assuming that $n_{\mathrm{N,AS}}/n_{\mathrm{O,AS}}$ is fixed and equal to that of the normal atmospheric air at sea level (i.e. 3.76), the partial pressures of nitrogen and oxygen in the cathode channel can be obtained from the known total pressure of the cathode channel. Thus, the steady-state values of the partial pressures of the gas species at the anode and the cathode gas channels are derived as functions of the SOFC operating conditions such as the temperature, the anodic and cathodic pressures, the load current, the FU and the OU. Therefore, it is possible to simulate the steady-state operation of the SOFC with the desired operating conditions.

Static characteristics of a fuel cell system are used to determine its operating regime. The partial pressures of the hydrogen and water vapour in the anode channel are set to obtain desired FU, i.e. $p_{\mathrm{H}}/p_{\mathrm{W}} = (1 - \zeta_{\mathrm{f}})/\zeta_{\mathrm{f}}$. The OU is set to zero (i.e. there is sufficient air flow such that the rate of oxygen consumption in the reactions can be neglected). This is achieved by setting the partial pressures of nitrogen and oxygen in the cathode channel in such a way that $p_{\mathrm{N}}/p_{\mathrm{O}}$ is equal to the ratio 0.79/0.21, which is the same ratio as in the normally available atmospheric air.

The initial partial pressures of the constituent gases, the initial temperatures of the mixture and the volume of the channels are the input parameters of the C-fields. The initial masses of the constituent gases are calculated from these inputs by using the ideal gas law. For example, the initial mass of hydrogen in the anode channel is given by

$$m_{\mathrm{H}}^{0} = \frac{p_{\mathrm{H}}^{0} V_{\mathrm{an}}}{R_{\mathrm{H}} T_{\mathrm{an}}^{0}} \tag{10.69}$$

where the value of p_{H}^{0} is known from the calculations discussed earlier (refer to (10.65)) and T_{an}^{0} is the desired steady-state temperature. The initial masses of other gas species are similarly calculated. The initial entropy of the anode channel gas mixture (hydrogen and water vapour) is calculated as

$$S_{\mathrm{an}}^{0} = S_{\mathrm{H}}^{\mathrm{ref}} + S_{\mathrm{W}}^{\mathrm{ref}} + \ln \left\{ \begin{array}{l} \left(\dfrac{T_{\mathrm{an}}^{0}}{T_{\mathrm{an}}^{\mathrm{ref}}} \right)^{m_{\mathrm{H}}^{0} c_{\mathrm{v,H}} + m_{\mathrm{H}}^{0} R_{\mathrm{H}} + m_{\mathrm{W}}^{0} c_{\mathrm{v,W}} + m_{\mathrm{W}}^{0} R_{\mathrm{W}}} \\ \left(\dfrac{p_{\mathrm{H}}^{\mathrm{ref}}}{p_{\mathrm{H}}^{0}} \right)^{m_{\mathrm{H}}^{0} R_{\mathrm{H}}} \left(\dfrac{p_{\mathrm{W}}^{\mathrm{ref}}}{p_{\mathrm{W}}^{0}} \right)^{m_{\mathrm{W}}^{0} R_{\mathrm{W}}} \end{array} \right\} \tag{10.70}$$

and the initial entropy of the cathode channel gas mixture (oxygen and nitrogen) is calculated in a similar manner. The values of all entropies at reference states are obtained from tables [2]. The initial entropy of the element C_M representing the thermal capacity of the MEA is given as

$$S_M^0 = S_M^{ref} + m_M c_M \ln\left(\frac{T_M^0}{T_M^{ref}}\right) \tag{10.71}$$

and the initial entropies of the capacitance elements C_{I1} and C_{I2} are also initialised in similar fashion.

10.3.2 Static Characteristics

The simulations were performed using the software SYMBOLS Shakti^{TM}[10]. The readers may refer to [12, 13, 15] for the parameters used in the simulations.

In Fig. 10.6, the polarisation and power density curves obtained from the model are compared with the data from [1] in which the fuel considered was CH_4 and the fuel composition for obtaining the static characteristic curves was fully reformed steam and methane mixture. It can be seen that the difference between the results is small because the principal gaseous species in the anode channel are still H_2 and H_2O, which is a valid assumption. A part of the small difference between the results can also be attributed to the difference in the calculations of the activation over-voltage between this model and [1].

Figure 10.7 shows the reversible cell voltage as a function of the FU with the system pressure as the parameter. From these curves, it is evident that the reversible cell voltage decreases with the increase in the FU and also that increasing system pressure results in increased Nernst voltage. However, this increase is quite small.

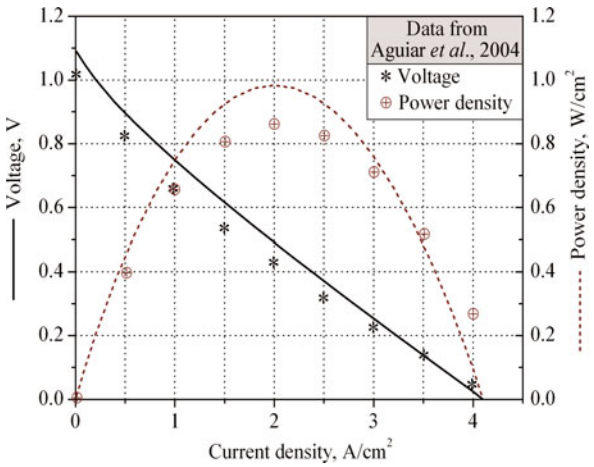

Fig. 10.6 Polarisation and power density curves of the SOFC

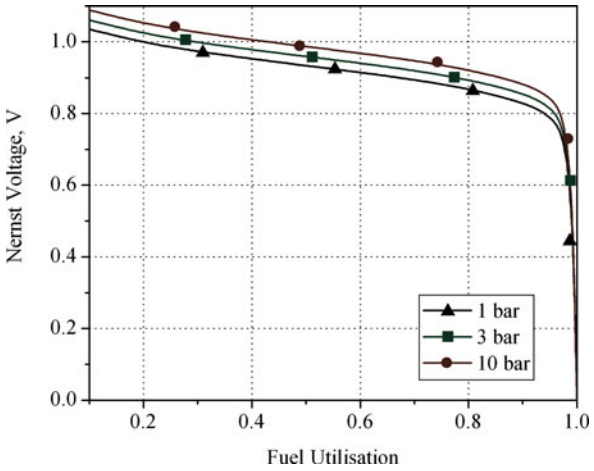

Fig. 10.7 Characteristic curves showing the variation of Nernst voltage as a function of FU

Moreover, high-pressure operation may lead to other complications. Therefore, the cell pressure is kept slightly above the atmospheric pressure. It can also be seen that the reversible cell voltage drops significantly for FUs near the value of unity. That is why, a FU of more than 0.9 is normally not desired. On the other hand, a low FU is economically unviable. Some other static characteristic curves of the SOFC can be referred to in [12, 13, 15].

10.3.3 Dynamic Responses

The dynamic response of the fuel cell to a step change in the load current is shown in Fig. 10.8. The dynamic response study helps us in understanding the various physical processes involved in the functioning of the fuel cell and ultimately guides us in developing efficient control strategies to improve SOFC system's load following capability.

The valve coefficients for the four valves are fixed at the values given by (10.63), (10.64), (10.66) and (10.67) to obtain the open-loop dynamic response of the SOFC. Step changes are made in the load current from 100 to 80 A at 500 s and from 80 to 90 A at 2000 s. The dynamic responses of the cell voltage, current, FU and OU to the step changes of load current, the data being normalised with respect to the initial steady-state conditions (Voltage $=$ 0.609036 V, Current $=$ 100 A, FU $=$ 0.8 and OU $=$ 0.125), are shown in Fig. 10.8a.

When the current is decreased, the combined effect of the changes in the partial pressures and the polarisation losses results in the increase of the cell voltage. It is observed that the cell voltage initially overshoots before settling to a steady-state value. The FU and the OU, which are proportional to the current, also decrease. The reverse phenomena are observed with the increase in the external load current. The sudden decrease in the load current results in the decrease in the rate of hydrogen and oxygen consumption and the rate of water vapour formation. In other words, the

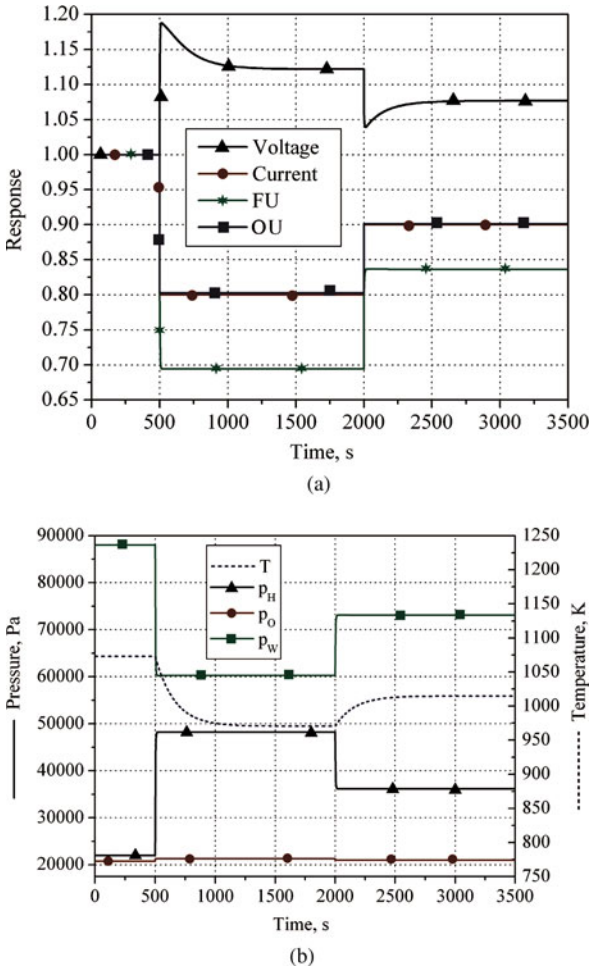

Fig. 10.8 Dynamic response curves for **(a)** voltage, current, FU and OU normalised to their initial values and **(b)** species partial pressures and cell temperature

reaction rate decreases. This results in the accumulation of hydrogen and oxygen in the chambers and hence their partial pressures increase almost abruptly. At the same time, the partial pressure of water vapour falls, as shown in Fig. 10.8b.

The decrease in the current also results in the decrease in the polarisation losses and the decrease in the reaction entropy flow rate ($\dot{S}_r$) (due to reduced mass flow rates) and thereby results in the fall of the system temperature. The reverse phenomena are observed (at time 2000 s in Fig. 10.8) when the load current density is increased.

It can be seen from Fig. 10.8b that the hydraulic (pressure) dynamics is much faster than the thermal (temperature) dynamics. Although the entropy flow due to the ohmic losses and the reaction is directly proportional to the current, the entropy flow due to the activation and concentration losses depends upon the gas species partial pressures. Therefore, the change in the heat production does not happen

instantaneously with the change in the current. Further, the solid components of the SOFC have high thermal capacities. Due to these reasons, it usually takes a long time (in the order of several minutes) for the cell temperature to settle down to a steady-state value after a disturbance. On the other hand, the pressure dynamics is faster due to the reason that the changes in the inlet and outlet mass flow rates are fast (only the small time delay associated with valve actuation, which is not modelled in this work, can affect it).

10.4 Conclusions

The systematic development of a zero-dimensional true bond graph model of a SOFC by using the concepts of network thermodynamics was presented in this chapter. A C-field for representing the energy storage in a two-species gas mixture is formulated, which is used in the construction of a bond graph model of the SOFC. An R-field formulation for representing the convection in two-species gas mixtures was also presented. The couplings between the various energy domains in a fuel cell system have been represented in a unified manner by using the true bond graphs. The developed model ensures energy balance at all physical process interfaces, e.g. entropy generation due to mixing, entropy generation due to heat transfer, charge transport and diffusion phenomena. The true bond graph model presented in this chapter clearly exposes the physical structure and process dynamics of the SOFC.

The developed model will be useful in designing integrated model-based control strategies for the overall system by including the load and power conditioning components. Moreover, various other control theoretic tools, fault detection algorithms and fault tolerant and robust control algorithms can be readily applied to the bond graph model. Because this model is based on the second law of thermodynamics of the system and the principles of network thermodynamics, it can be used for performing exergy-based system optimisation studies.

The model is properly initialised and simulations are performed to obtain the static characteristics and dynamic responses of the SOFC. For obtaining the static characteristic curves of the SOFC, the FU and the OU have been interpreted in terms of the partial pressures of the gas species in the channels, for a given set of known and input parameters. The application of the true bond graph model presented in this chapter for the optimisation of the operational efficiency of a SOFC system consisting of the cell, the after-burner and two pre-heaters under varying loads can be consulted in [12, 14, 16]. Readers may also refer to [12, 15] for a control scheme to improve the dynamic performance of the SOFC using the true bond graph model presented in this chapter.

Acknowledgements The first author would like to acknowledge Prof. Moses Tadé, Dean of Engineering, Curtin University of Technology, for kindly permitting him to write this chapter during his stay as a research associate at the University.

References

1. Aguiar P, Adjiman CS, Brandon (2004) Anode-supported intermediate-temperature direct internal reforming solid oxide fuel cell I. Model-based steady-state performance. J Power Sources 138: 120–136.
2. Benson RS (1977) Advanced Engineering Thermodynamics, 2nd ed. Pergamon Press Limited, Oxford.
3. Bockris JO'M, Reddy AKN, Gamboa-Aldeco M (1998) Modern Electrochemistry: Fundamentals of Electrodics, 2nd ed. Kluwer/Plenum, Dordrecht.
4. Breedveld PC (1984) Physical Systems Theory in Terms of Bond Graphs. Ph.D. Thesis, Twente University, Enschede.
5. Callen HB (1985) Thermodynamics and an Introduction to Thermostatistics. Wiley, New York, NY.
6. Feenstra PJ (2000) A Library of Port-Based Thermo-Fluid Submodels. M.Sc.Thesis, University of Twente.
7. Karnopp DC, Margolis DL, Rosenberg RC (2006) System Dynamics: Modeling and Simulation of Mechatronic Systems, 4th ed. Wiley, Hoboken, NJ.
8. Mukherjee A, Karmakar R, Samantaray AK (2006) Bond Graph in Modeling, Simulation and Fault Identification. CRC Press, Boca Raton, FL.
9. Perelson AS (1975) Network thermodynamics, an overview. Biophys J 15: 667–685.
10. Samantaray AK, Mukherjee A (2006) Users Manual of SYMBOLS Shakti. (High-Tech Consultants, STEP, Indian Institute of Technology, Kharagpur, <http://www.htcinfo.com/>)
11. Thoma J, Ould Bouamama B (2000) Modelling and Simulation in Thermal and Chemical Engineering. Springer, New York, NY.
12. Vijay P (2009) Modelling, Simulation and Control of a Solid Oxide Fuel Cell System: A Bond Graph Approach. Ph.D. Thesis, Indian Institute of Technology, Kharagpur, India.
13. Vijay P, Samantaray AK, Mukherjee A (2008) Bond graph model of a solid oxide fuel cell with a C-field for mixture of two gas species. Proc IMechE, Part I: J Syst Control Eng 222(4): 247–259.
14. Vijay P, Samantaray AK, Mukherjee A (2009) On the rationale behind constant fuel utilization control of solid oxide fuel cells. Proc IMechE, Part I: J Syst Control Eng 223(2): 229–252.
15. Vijay P, Samantaray AK, Mukherjee A (2009) A bond graph model-based evaluation of a control scheme to improve the dynamic performance of a solid oxide fuel cell. Mechatronics 19(4): 489–502.
16. Vijay P, Samantaray AK, Mukherjee A (2010) Constant fuel utilization operation of a SOFC system: An efficiency viewpoint. Trans ASME J Fuel Cell Sci Technol 7(4): 041011 (7 pages).
17. Vijay P, Samantaray AK, Mukherjee A (2010) Parameter estimation of chemical reaction mechanisms using thermodynamically consistent kinetic models. Comput Chem Eng 34(6): 866–877.
18. Zemansky MW, Dittman DH (1997) Heat and Thermodynamics. McGraw-Hill, Singapore.